Thermal expansion of iron-rich alloys and implications for the Earth's core

Bin Chen*†, Lili Gao*, Ken-ichi Funakoshi‡, and Jie Li*

*Department of Geology, University of Illinois at Urbana–Champaign, 1301 West Green Street, Urbana, IL 61801; and ‡Japan Synchrotron Radiation Research Institute, SPring-8, Hyogo 679-5198, Japan

Edited by Ho-Kwang Mao, Carnegie Institute of Washington, Washington, DC, and approved November 28, 2006 (received for review September 5, 2006)

Understanding the thermal–chemical state of the Earth's core requires knowledge of the thermal expansion of iron-rich alloys at megabar pressures and high temperatures. Our survey of literature revealed a significant lack of such data. We have determined the unit-cell parameters of the iron–sulfur compound Fe_3S by using synchrotron x-ray diffraction techniques and externally heated diamond–anvil cells at pressures up to 42.5 GPa and temperatures up to 900 K. The zero-pressure thermal expansivity of Fe_3S is determined in the form $\alpha = a_1 + a_2T$, where $a_1 = 3.0 \pm 1.3 \times 10^{-5}$ K^{-1} and $a_2 = 2.8 \pm 1.5 \times 10^{-8}$ K^{-2}. The temperature dependence of isothermal bulk modulus $(\partial K_{T,0}/\partial T)_P$ is estimated at $-3.75 \pm 1.80 \times 10^{-2}$ GPa K^{-1}. Our data at 42.5 GPa and 900 K suggest that ≈2.1 at. % (1.2 wt. %) sulfur produces 1% density deficit in iron. We have also carried out energy-dispersive x-ray diffraction measurements on pure iron and $Fe_{0.864}Si_{0.136}$ alloy samples that were placed symmetrically in the same multianvil cell assemblies, using the SPring-8 synchrotron facility in Japan. Based on direct comparison of unit cell volumes under presumably identical pressures and temperatures, our data suggest that at most 3.2 at. % (1.6 wt. %) silicon is needed to produce 1% density deficit with respect to pure iron.

Fe_3S | Fe–Si alloy | light element

The Earth's core makes up nearly one third of the planet's mass. Its composition, property, and dynamics are fundamental issues in the study of the Earth's interior. Deeply buried in the center of the planet, the core has kept its chemical composition a long-standing mystery. Cosmochemical studies of meteorites and geochemical analysis of samples from shallower portions of the Earth suggest that the core is made of iron (Fe)-rich alloys containing nickel (Ni) and one or more lighter elements (1). A critical test for any candidate core composition model is that it must be able to reproduce the physical properties of the core. On the basis of observing seismic rays penetrating the deep interior of the Earth and the orbital dynamics of the Earth as a planet in the solar system, models have been constructed to describe the physical state, density profile, and velocity profiles of the Earth's interior. One of the most widely used models is PREM (2). To perform the test of consistency between a composition model and the PREM model, we must know the thermal state of the core and the equation-of-state (EOS) of various Fe-rich alloys at the pressure and temperature conditions of the core. The thermal state of the core can be deduced from the freezing point of core composition at the pressure of inner–outer core boundary and the adiabatic temperature gradient of the core composition under core pressures through laboratory measurements. Uncertainties in the core composition directly lead to uncertainties in the thermal state. By iteration, a self-consistent model of the thermal–chemical state of the core may be found. To complement this approach, we need accurate and precise phase relation and EOS data of various Fe-rich alloys at megabar pressures and high temperatures. In this paper, we review existing data on the thermal expansion of Fe-rich alloys and report experimental data on thermal expansion of Fe_3S, Fe, and Fe–Si alloys.

Thermal Expansion of Fe-Rich Alloys Under Static High Pressure: A Survey

Thermal expansion is a fundamental aspect of EOS. Various parameters have been introduced to characterize thermal expansion under elevated pressures. They fall into two general categories, one focusing on macroscopic thermodynamic quantities and derivatives, and the other based on lattice vibration theories and microscopic view of solids. In the first category, P–V–T data are grouped into isothermal, isobaric, or isochoric sets. A basic approach is to calculate the thermal expansion coefficient from isobaric data according to its definition $\alpha = (\partial \ln V/\partial T)_P$. The temperature dependence of thermal expansion coefficient is normally expressed in the form of $\alpha = a_1 + a_2T$ or $\alpha = a_1 + a_2T + a_3T^{-2}$ (e.g., ref. 3). One can also calculate temperature-dependent bulk modulus $(\partial K_{T,0}/\partial T)_P$ by fitting isothermal data to the high-temperature Birch–Murnaghan EOS. Isochoric data allow the calculation of thermal pressure at constant volume, which is related to thermal expansion coefficient and isothermal bulk modulus: $\Delta P_{\text{thermal}} = \alpha K_T \Delta T$, where αK_T is commonly assumed to be constant at temperatures above the Debye temperature. In the second category, the Mie–Grüneisen–Debye EOS is widely used to extract a number of thermoelastic parameters from P–V–T data, including the isothermal bulk modulus at ambient pressure ($K_{T,0}$), its pressure derivative ($K'_{T,0}$), the Debye temperature at ambient pressure and temperature θ_0, the Grüneisen parameter γ_0 (which describes the volume dependence of the Debye temperature), and q (which is a parameter describing the volume dependence of the Grüneisen parameter). Jackson and Rigden (4) carried out a systematic analysis of P–V–T data of mantle minerals and found excellent agreements between different methods.

A survey of literature revealed a significant lack of thermal expansion data on Fe-rich alloys under static high pressure (Table 1). Extensive efforts have been focused on pure Fe. With the recent development in high-pressure and high-temperature experimental techniques and concurrent advance in synchrotron radiation facilities, this simplified core composition model has become amenable to investigations under increasingly higher pressures and temperatures. Using diamond–anvil cells and internal heating technique, Dubrovinsky *et al.* (5, 6) determined the thermal expansion of Fe to a maximum pressure of 300 GPa and a maximum temperature of 1,500 K. Two multianvil studies covered similar range of temperature at moderate pressures (7, 8). An independent estimate of the Debye temperature has been

Author contributions: B.C., L.G., and J.L. performed research; K.-i.F. contributed new reagents/analytic tools; B.C., L.G., and J.L. analyzed data; and B.C., L.G., and J.L. wrote the paper.

The authors declare no conflict of interest.

Abbreviations: EOS, equation-of-state; hcp, hexagonal close-packed.

†To whom correspondence should be addressed at: Department of Geology, University of Illinois at Urbana–Champaign, 1301 West Green Street, Urbana, IL 61801. E-mail: binchen2@uiuc.edu.

This article contains supporting information online at www.pnas.org/cgi/content/full/0610474104/DC1.

Table 1. Thermal expansion data of Fe and Fe-rich alloys

Phase	P, T coverage	Parameters	Ref.
Fe (ε)	0–20 GPa, 298–1,500 K	$a_1 = 3.98(25) \times 10^{-5}$ K^{-1}*	8
		$a_2 = 5.07(88) \times 10^{-8}$ K^{-2}	
		$(\partial K_{T,0}/\partial T)_P = -4.48(56) \times 10^{-2}$GPa K^{-1}†	
		$\alpha K_T = 6.88(30) \times 10^{-3}$ GPa K^{-1}‡	
		$(\partial^2 P/\partial T^2)_V = 4.63(53) \times 10^{-6}$ GPa K^{-2}	
		$\theta_0 = 998(85)$ K, $\gamma_0 = 1.36(8)$, $q = 0.91(7)$§	
	0–153 GPa, 300 K	$\theta_0 = 420$ K§	9
	19–285 GPa, 300–1,250 K	$\theta_0 = 430(3)$ K, $\gamma_0 = 1.78$ (6), $q = 0.69(10)$§	10
	0–300 GPa, 300–1,300 K	$\alpha_0 = 6.93(37) \times 10^{-5}$ K^{-1}*	6
	0–68 GPa, 300–1,500 K	$a_1 = 5.7(4) \times 10^{-5}$ K^{-1}*	5
		$a_2 = 4.2(4) \times 10^{-9}$ K^{-2}	
		$a_3 = -0.17(7)$ K	
	22–32 GPa, 300–1,500 K	$\alpha = 3.88 \times 10^{-5}$ K^{-1} (22 GPa)*	7
		$\alpha = 3.16 \times 10^{-5}$ K^{-1} (32 GPa)	
Fe_3S	0–43 GPa, 300–900 K	$a_1 = 3.0(1.3) \times 10^{-5}$ K^{-1}*	This study
		$a_2 = 2.8(1.5) \times 10^{-8}$ K^{-2}	
	0–80 GPa, 300–2,500 K	$\alpha K_T = 0.011(2)$ GPa K^{-1}‡	17
$Fe_{0.84}Si_{0.16}$	0–8.9 GPa, 300–773 K	$\alpha_0 = 4.74(17) \times 10^{-5}$ K^{-1} ($K_{T,0}' = 4$)*	19
		$\alpha_0 = 4.90(18) \times 10^{-5}$ K^{-1} ($K_{T,0}' = 5.3$)	
FeSi	1 bar, 4–1,173 K	$\theta_0 = 445(11)$ K, $\gamma_0 = 2.33(3)$§	20
	0–10 GPa, 300–1,073 K	$\alpha_0 = 5.10(40) \times 10^{-5}$ K^{-1}*	18
Fe_3C	1 bar, 4–600 K	$\alpha_0 = 4.1$ (1) $\times 10^{-5}$ K^{-1}($>T_c$)*	21
		$\alpha_0 < 1.8(1) \times 10^{-5}$ K^{-1} ($<T_c$)	

*Thermal expansion coefficient according to its definition. $V_0(T) = V_0\exp(\int_{300}^{T} \alpha_0 dT)$, where V_0 (300 K) is the unit cell volume at 1 bar and 300 K, α_0 is the thermal expansion coefficient at 1 bar. It is normally expressed in the form of $\alpha_0(T) = a_1 + a_2T$ or $\alpha_0(T) = a_1 + a_2T + a_3T^{-2}$.

†Temperature-dependent isothermal bulk modulus (K_T) based on high temperature Birch–Murnaghan EOS.

‡Thermal pressure EOS based on Mie–Grüneisen theory. $\Delta P_{\text{thermal}} = \alpha K_T \Delta T$, where αK_T is constant.

§Mie–Grüneisen–Debye EOS, where θ_0 is the Debye temperature at 1 bar and 300 K, γ_0 is the Grüneisen parameter describing the volume dependence of the Debye temperature, and q is a parameter describing the volume dependence of the Grüneisen parameter above the Debye temperature.

obtained from nuclear resonant inelastic scattering measurements, which determined the phonon density of states of Fe up to 153 GPa and at ambient temperature (9). The Debye temperature at 1 bar derived from the phonon density of sta tes data agrees well with that from a x-ray diffraction study in a diamond–anvil cell (420–430 K) (10), but they are in stark disagreement with the result of multianvil experiments (≈1,000 K) (8). All of the reported thermal expansion coefficients at ambient conditions agree within uncertainties. Although laser-heated diamond anvil cells have been used extensively to determine the structural phase transition of Fe, no thermal expansion data have been reported. Due to limited temperature range covered by the existing static experiments, current discussions concerning the effect of thermal expansion on the density deficit in the Earth's core have largely relied upon shock wave data (11, 12).

The leading candidates for alloying elements in the Earth's core include Ni, sulfur (S), silicon (Si), carbon (C), oxygen (O), and hydrogen (H) (see reviews in refs. 13–16). The phase relations and thermoelastic properties of a number of binary systems including Fe and one of the alloying elements have been studied under high pressures and temperatures. We found that thermal expansion data for Fe-rich alloys are extremely limited. With laser-heated diamond–anvil cells, thermal EOS of Fe_3S has been measured to 80 GPa and 2,500 K (17). High-pressure data on Fe–Si alloys were collected in multianvil apparatus at pressures below 10 GPa (18, 19). Two studies were conducted at ambient pressure using neutron diffraction method, one on Fe_3C and the other on FeSi (20, 21). In general, the thermal expansion coefficients at ambient conditions are lower than that of pure Fe by >20%, with that of Fe_3C being the lowest. It is clear that more thermal expansion data are needed to evaluate the effects of alloying elements on the thermoelastic properties of Fe.

Experimental Results and Discussion

Thermal Expansion of Fe_3S. In Fe-S binary system, Fe_3S with 16.1 wt.% S is the most Fe-rich sulfide known to date. Fe_3S belongs to the tetragonal crystal system with space group $I\bar{4}$ and is isostrucutral with Cr_3P (22). The unit-cell parameters of Fe_3S at ambient condition are $a = 9.144(2)$ and $c = 4.509(2)$ Å, with a zero-pressure density of 7.033 g/cm^3. Our x-ray diffraction patterns are consistent with this structure model, indicating no structural phase transition up to 42.5 GPa and 900 K. The volume-pressure data of Fe_3S at temperatures of 300, 600, and 900 K have been determined under pressures up to 42.5 GPa [see Fig. 1*a* and supporting information (SI) Table 2]. The high-temperature Birch–Murnaghan EOS (ref. 23 and references therein) is used to fit the isothermal compressional data

$$P(V) = \frac{3}{2} K_{T,0}\left[\left(\frac{V_0}{V}\right)^{\frac{7}{3}} - \left(\frac{V_0}{V}\right)^{\frac{5}{3}}\right] \times \left\{1 - \frac{3}{4}(4 - K_{T,0}')\left[\left(\frac{V_0}{V}\right)^{\frac{2}{3}} - 1\right]\right\}, \quad [1]$$

where $K_{T,0}$, $K_{T,0}'$, and V_0 are the bulk modulus, its pressure derivative, and the unit cell volume at zero pressure and temperature T, respectively. The room-pressure unit cell volume V_0 is given by the following expression: $V_{0(T)} = V_0$ (300 K) $\exp(\int_{300}^{T} \alpha_{T,0} dT)$, where V_0 and $\alpha_{T,0}$ are the unit cell volume at room pressure and 300 K and the thermal expansion coefficient

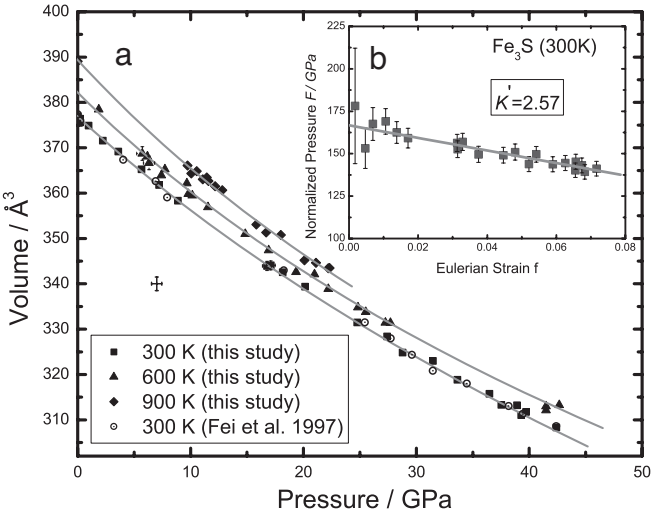

Fig. 1. Isothermal compression data of Fe_3S at 300, 600, and 900 K. (*a*) Open circles represent compression data at room temperature (300 K) from Fei *et al.* (22). Filled squares, triangles, and diamonds represent the compression data at 300, 600, and 900 K, respectively. The three lines are the third-order Birch–Murnaghan EOS fits to the compression data. The error bars are estimated from multiple x-ray measurements at the same condition. Where duplicate measurements were not made, uncertainties estimated from multiple diffraction lines in a single measurement are slightly smaller than the symbols. A typical error bar is shown in the lower left corner. (*b*) $f - F$ plot of the compression data at 300 K. The data can be fitted by an inclined straight line, suggesting that the compression of Fe_3S can be adequately described by a third-order Birch–Murnaghan EOS. The error bars are based on multiple diffraction lines in a single measurement.

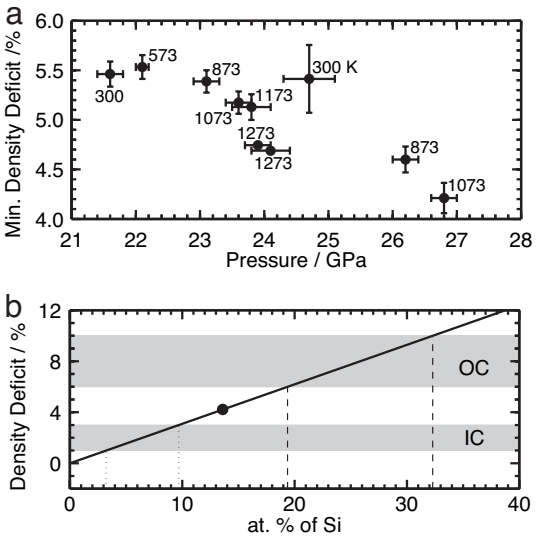

Fig. 2. Density deficits in Fe–Si alloys and Si content in the Earth's core. (*a*) Minimum density deficit between hcp–$Fe_{0.864}Si_{0.136}$ and hcp–Fe under different experimental conditions. Density deficit is defined as $(1 - \rho_{Fe\text{-}Si}/\rho_{Fe}) \times 100\%$, where ρ represents the density. These data are listed in SI Table 4. Numbers next to symbols denote temperatures in Kelvin. (*b*) Density deficit versus maximum Si content in Fe–Si alloy with hcp structure. Gray regions labeled "OC" and "IC" indicate density deficit of the outer and inner core compared with pure Fe, respectively (ref. 16 and references therein). The filled circle represents the minimum density deficit produced by 13.6 at. % Si, based on data in *a*. The solid line represents a linear relationship between density deficit and Si content; dotted and dashed lines enclose the ranges of maximum Si content in the IC and OC, respectively.

at room pressure and temperature T, respectively. Results of the least-squares fit of the third-order Birch–Murnaghan EOS to the compression data are plotted in Fig. 1*a* (see SI Table 3). The $f - F$ plot (Fig. 1*b*) confirmed that the compression data of Fe_3S are adequately described by a third-order truncation of EOS (ref. 23 and references therein). The temperature dependence of isothermal bulk modulus $(\partial K_{T,0}/\partial T)_P$ is estimated at $-3.75 \pm 1.80 \times 10^{-2}$ GPa K^{-1}. We calculated the thermal expansion coefficients of Fe_3S at 1 bar. Assuming a linear temperature dependence in the form of $\alpha_{T,0} = a_1 + a_2T$, we found $a_1 = 3.0 \pm 1.3 \times 10^{-5}$ K^{-1} and $a_2 = 2.8 \pm 1.5 \times 10^{-8}$ K^{-2}.

Fei *et al.* (22) determined the compression curve of Fe_3S at 300 K. They reported isothermal bulk modulus $K_{T,0} = 170(8)$ GPa with a corresponding pressure derivative $K'_{T,0} = 2.6(5)$ or $K_{T0} = 150(2)$ GPa with fixed $K'_{T,0} = 4$. Seagle *et al.* (17) extended the thermal EOS of Fe_3S to 80 GPa and 2,500 K and determined the bulk modulus of Fe_3S at room temperature $K_{T,0} = 156(7)$ GPa with pressure derivative $K'_{T,0} = 3.8(3)$ by fitting a third-order Birch–Murnaghan EOS to room temperature compression data by using NaCl in B2 structure as a pressure scale. They also reported $\alpha K_T = 0.011$ (2) GPa K^{-1} for Fe_3S, by expressing the thermal contribution of Fe_3S in the form of $\Delta P_{thermal} = \alpha K_T \Delta T$. The α_0 calculated from $\alpha K_T = 0.011(2)$ GPa K^{-1} and $K_{T0} = 113(9)$ given in Seagle *et al.* (17) is significantly higher than our results. The discrepancy may result from the temperature dependence of thermal expansion coefficient. Extrapolating our calculated thermal pressures at 600 and 900 K to higher temperatures, our trend agrees with that in Seagle *et al.* (17) within experimental uncertainties, but falls within the negative side of their error bars.

Thermal Expansion of Fe and Fe–Si Alloys. Pairs of x-ray diffraction measurements were taken on both pure Fe and an $Fe_{0.864}Si_{0.136}$ sample in the same cell assembly, within the pressure range of 21–27 GPa and the temperature range of 300 to >2,000 K. Within this pressure range and between 300 and 1,273 K, Fe adopts the hexagonal close-packed (hcp) structure, whereas $Fe_{0.864}Si_{0.136}$ breaks down to a mixture of a Si-enriched body-centered cubic phase and a Si-depleted hcp phase (24). These are proposed to be the stable forms of Fe and Fe–Si alloy in the Earth's inner core. At higher temperatures, the hcp–Fe phase disappears; thus, data collected at temperatures above 1,273 K are not reported here. Calculated minimum density deficit of hcp–$Fe_{0.864}Si_{0.136}$ relative to hcp–Fe from the paired data are shown in Fig. 2. Because the hcp phase of Fe–Si alloy contains less Si than the starting material, these values represent lower limits of density deficits caused by 13.6 at. % Si. The variations in density deficit reflect varying Si content in the Fe–Si alloys as a function of pressure and temperature and the differences in compressibility and thermal expansion between the Fe–Si alloys and pure Fe.

Most existing EOS measurements are performed on individual phases for the sake of minimizing interference in x-ray diffraction spectra and possible chemical reactions. Any discrepancies in pressure and temperature between separate experiments would introduce uncertainties to the calculated density deficit. Direct comparison of densities between an Fe-rich alloy and pure Fe under identical conditions has the advantage of eliminating or reducing such uncertainties. The technique of measuring symmetrically placed samples in a multianvil apparatus was pioneered by Zhang and Guyot (19). That of measuring well mixed samples in a laser-heated diamond–anvil cell was first applied by Seagle *et al.* (17). In this study, we have extended the pressure range of such multianvil investigation from <10 GPa to nearly 30 GPa. Our data place a lower limit on the capability of Si to reduce the density of solid Fe. Further constraints can be obtained by carrying out chemical analysis of run products quenched from each temperature and pressure conditions.

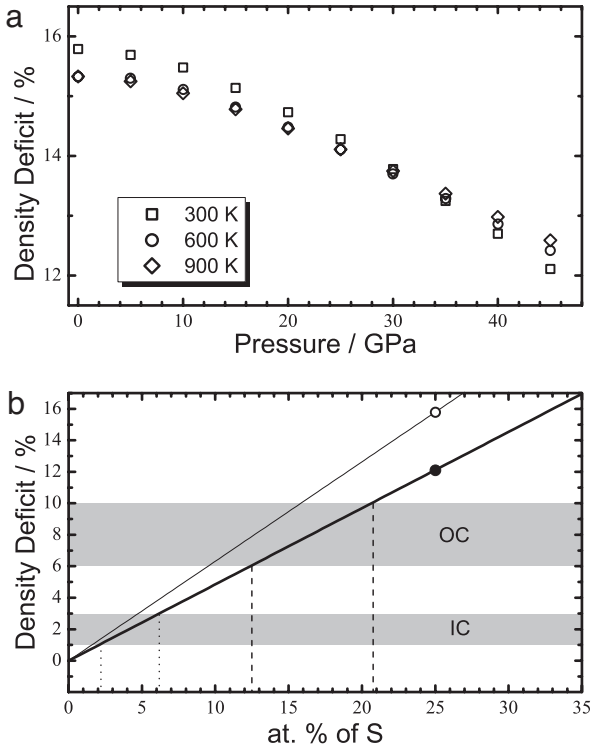

Fig. 3. Density deficit in Fe_3S and S content in the Earth's core (*a*) Density deficit between Fe_3S and Fe, $(1 - \rho_{Fe3S}/\rho_{Fe}) \times 100\%$ versus pressure. (*b*) Density deficit versus S content in an Fe–S alloy. The open circle denotes the density deficits of Fe_3S with respect to Fe at 1 bar and 300 K. The filled circle denotes the deficits at 42.5 GPa and 900 K. Gray regions labeled ''OC'' and ''IC'' indicate density deficits of the outer and inner core with respect to pure Fe, respectively (ref. 16 and references therein). The solid lines represent linear relationships between density deficit and S content; dotted and dashed lines enclose the ranges of S contents in the IC and OC, respectively.

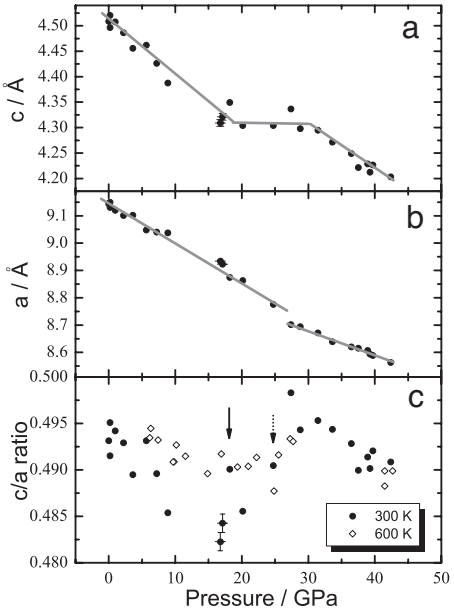

Fig. 4. Lattice parameters of Fe_3S versus pressure at 300 and 600 K. (*a*) Lattice parameter *c* versus pressure at 300 K. (*b*) Lattice parameter *a* versus pressure at 300 K. (*c*) *c*/*a* ratio versus pressure at 300 and 600 K. For clarity, the *c* and *a* data at 600 K are not shown. The solid arrow indicates the valley in the 300 K data. The dotted arrow indicates the valley in the 600 K data. The error bars are estimated from multiple x-ray measurements.

Light Element Contents of the Core. Geochemical and cosmochemical observations suggest that S is a major component of terrestrial and Martian cores (e.g., refs. 25–28). Previous estimates of the amount of S needed to account for the outer core density deficit range from a few weight percent to as much as 18 weight percent (14, 16, 17, 26, 29, 30). The Earth's core probably has a S content between pure Fe and Fe_3S. Given a higher S content in Mars, Fe_3S is a possible component of the Martian inner core. To estimate the core's S content based on our new data, we calculated the density deficit of Fe_3S with respect to pure Fe as a function of pressure and temperature. The deficit decreases with pressure (see Fig. 3*a*), suggesting that Fe_3S is more compressible than Fe. Within the experimental pressure and temperature range, the temperature effect on the density deficit is not as significant as that of pressure (Fig. 3*a*). Assuming a linear relationship between density deficit and S content, we estimated that at ambient conditions ≈1.6 at. % (0.9 wt. %) S can produce 1% density deficit (Fig. 3*b*). At 45 GPa and 900 K, ≈2.1 at. % (1.2 wt. %) S is needed to produce the same amount of density deficit (Fig. 3*b*). Extrapolating our data based on Birch–Murnaghan EOS to the core conditions leads to unreasonable results, probably due to uncertainties in the fitted K_T' values. Given 6–10% deficit between the outer core and solid Fe, and 1–3% deficit between the inner core and solid Fe (ref. 16 and references therein), we estimated 12.5–20.7 at. % (7.6–13.0 wt. %) S in the outer core and 2.2–6.2 at. % (1.3–3.7 wt. %) S in the inner core based on our data at the highest experimental pressure and temperature. Implicit in the estimated S content in the outer core is the assumption that S has a negligible effect on the volume change across the liquid–solid boundary.

Si is among the top three most abundant elements in the Earth's crust and mantle. A considerable amount of Si may be incorporated into the core through chemical reactions, especially under reducing conditions (31, 32). Geochemical data suggest that, depending on the accretion history and the distribution of Si in various layers inside the Earth, the Si content of the core may vary between virtually zero to 14 wt. % (31, 33, 34). Existing estimates of the amount of Si needed to account for 1% density deficit in the core range from 2.9 at. % (1.5 wt. %) to ≈5.8 at. % (3 wt. %) (18, 19, 24, 35). Assuming a linear relationship between density deficit and Si content, we estimated that, between 22.1 and 26.8 GPa, no more than 3.2 at. % (1.6 wt. %) Si is needed to produce 1% density deficit in hcp–Fe. This estimate agrees well with the lower estimate in the literature (19). Given 6–10% deficit between the outer core and solid Fe, and 1–3% deficit between the inner core and solid Fe (ref. 16 and references therein), our experimental data suggest an upper limit of 19–32 at. % (11–19 wt. %) Si in the outer core, and an upper limit of 3.2–9.6 at. % (1.6–5.1 wt. %) Si in the inner core.

K_T' and Velocity Gradient in the Outer Core. The fitting of our thermal EOS data to Fe_3S third-order Birch-Murnaghan EOS gives pressure derivative of bulk modulus $K_T' < 4$ (see SI Table 3), similar to the results of Fei *et al.* (22). Williams and Knittle (36) proposed that K_T' can place an effective constraint on the primary alloying element in the outer core. They concluded that a K_T' value that is <4 cannot reproduce the large gradient of bulk sound velocity in the outer core. Although their application of this constraint to Si was invalidated by later studies (e.g. refs. 18, 19, and 37), it is still a useful criterion for testing core composition models. If the small K_T' of Fe_3S persists to higher pressures and temperatures, the model of a S-rich core would be challenged. The K_T' from our study and Fei *et al.* (22) are much smaller than that given in Seagle *et al.* (17). Independent studies are needed to resolve the discrepancy.

Effect of Spin Transition. Fe-rich alloys may undergo pressure-induced high-spin to low-spin transitions. Magnetic transitions in pure Fe and troilite (FeS) are accompanied by structural phase transformation (38, 39), whereas those in Fe_3S and cementite (Fe_3C) do not seem to involve major structural changes (40, 41). *Ab initio* calculations of Fe_3C predicted abrupt volume reduction at the transition, which has not been observed in experiments (42). Nevertheless, such transition has been shown to affect the elastic and thermodynamic properties of Fe_3C and Fe_3S (40, 41). Without prior knowledge of the magnetic transition, fitted EOS may be erroneous.

At room temperature, the high- to low-spin transition in Fe_3S occurs between 20 and 25 GPa (40). Concurrent reduction in the unit-cell volume was not observed in our study. However, a plot of c/a ratio as a function of pressure revealed an obvious change between 20 and 27 GPa, with a valley located at ≈18 GPa (see Fig. 4*c*). This pressure range matches that of magnetic transition in Fe_3S. The change in c/a ratio results from an increased resistance along the c axis accompanied by a softened a axis, with little change in volume (Fig. 4). The data at 600 K suggest a similar but less obvious change in the c/a ratio between 25 and 28 GPa. The existence and condition of this change is poorly constrained due to the sparse data coverage. The observed c/a ratio change may be associated with the high- to low-spin transition of Fe_3S, unless it is fortuitously caused by redistribution of stress due to the B1–B2 transition in the NaCl pressure medium, which occurs within the same pressure range. To determine the spin state of Fe in a S-rich core, we need more measurements to cover a larger pressure range at high temperatures. Different pressure media should be used to avoid the interference from phase transition in NaCl.

Materials and Methods

Fe_3S. The starting material Fe_3S was synthesized stoichiometrically from metallic Fe and troilite (FeS) in a subsolidus experiment at 21 GPa and 1,000°C in a multianvil apparatus at Carnegie Institution of Washington. Electron microprobe and powder x-ray diffraction analysis indicate that the quenched run product is predominantly Fe_3S phase with <2% metallic Fe.

Energy-dispersive x-ray diffraction measurements were carried out by using polychromatic (white) wiggler synchrotron x-ray radiation at X17C beamline, the National Synchrotron Light Source, Brookhaven National Laboratory. The experimental procedure was similar to that described by Fei *et al.* (22). A germanium solid-state detector was used to collect the diffraction data at a fixed 2θ angle of 12.01°, which was calibrated by the x-ray diffraction spectrum of gold at ambient conditions. Two diamond–anvil cell assemblies were used for the measurements, both containing Fe_3S sample sandwiched between NaCl pressure medium. A small amount of MgO, Au, and Pt was placed next to the sample in one assembly, whereas only Au was included in the other.

An externally heated diamond–anvil cell was used to generate high pressures and temperatures (43). X-ray diffraction data were collected in several compression–heating–quench cycles covering pressures up to 42.5 GPa at 300, 600, and 900 K. Temperatures were measured with a platinum-rhodium (Pt-Rh) thermo-couple. The tetragonal unit-cell parameters for Fe_3S were fitted by using the GSAS/EXPGUI program (44, 45), primarily from the diffraction lines 321, 330, and 112. Typical diffraction patterns collected in this study are shown in SI Fig. 5. Pressures were primarily determined from Au pressure scale (46). NaCl was also used as a secondary pressure scale (47). Above the B1–B2 transition in NaCl at ≈29 GPa, pressures were calculated only from the lattice parameters of Au.

Fe and $Fe_{0.864}Si_{0.136}$. The experiments on Fe and $Fe_{0.864}Si_{0.136}$ (7.3 wt.% of Si) were carried out by using a Kawai-type multianvil press at the BL04B1 high-pressure and high-temperature beam line at the SPring-8 synchrotron facility in Japan. The experimental procedure was similar to that described by Fei *et al.* (48). In each run, we placed two samples symmetrically inside a cylindrical heater. One sample is a mixture of polycrystalline Fe (a few microns in average grain size, and >99.99% purity, from Goodfellow, Oakdale, PA) and MgO powder (99.99% purity, from Alfa Aesar, Ward Hill, MA) at a weight ratio of 1:4. MgO served as a pressure marker, and was also used to inhibit Fe crystal growth at high temperature. The other sample is a polycrystalline $Fe_{0.864}Si_{0.136}$ alloy from Goodfellow. The two samples were separated by a layer of packed MgO powder. In the first run, samples were first compressed to a target pressure of 800 tons (≈21 GPa). They were then annealed at 1,173 K to reduce nonhydrostatic stress, followed by a series of x-ray diffraction measurements along a heating ramp from room temperature to the peak temperature of 2,373 K. In the second run, a target pressure of 1,200 tons (≈25 GPa) and a peak temperature of 2,273 K were reached. Samples were annealed at 973 K. For the energy dispersive x-ray diffraction measurements, the solid state detector was fixed at an angle of 5.814° relative to the incident x-ray beam. The acquisition time for each spectrum is 200 s. The position of x-ray beam was monitored through an x-ray absorption image. X-ray diffraction spectra were analyzed by using the XRAYANA software provided by the beamline, and using the GSAS/EXPGUI (44, 45). Typical diffraction patterns collected in this study are shown in SI Fig. 6.

We thank Dr. Yingwei Fei for his contribution, Dr. Jingzhu Hu from Beamline X17C at National Synchrotron Light Source of Brookhaven National Laboratory for technical support, and Dr. Viktor Struzhkin for enlightening discussions. Thoughtful and constructive reviews by Dr. Jungfu Lin and Dr. Andrew Campbell improved the manuscript substantially. This work is supported by National Science Foundation Grants EAR-0337612 and EAR-0609639.

1. McDonough WF (2003) in *Treatise on Geochemistry*, ed Carlson RW (Elsevier, New York) Vol 2, pp 547–568.
2. Dziewonski AM, Anderson DL (1981) *Phys Earth Planet Inter* 25: 297–356.
3. Duffy TS, Wang Y (1998) in *Ultrahigh-Pressure Mineralogy: Physics and Chemistry of the Earth's Deep Interior*, ed Hemley RJ (Mineral Soc Am, Washington, DC), pp 425–457.
4. Jackson I, Rigden SM (1996) *Phys Earth Planet Inter* 96:85–112.
5. Dubrovinsky L, Saxena SK, Lazor P (1998) *Phys Chem Miner* 25:434–441.
6. Dubrovinsky LS, Saxena SK, Tutti F, Rekhi S (2000) *Phys Rev Lett* 84:1720–1723.
7. Funamori N, Yagi T, Uchida T (1996) *Geophys Res Lett* 23:953–956.
8. Uchida T, Wang YB, Rivers ML, Sutton SR (2001) *J Geophys Res* 106:21799–21810.
9. Mao HK, Xu J, Struzhkin VV, Shu J, Hemley RJ (2001) *Science* 292: 914–916.
10. Dubrovinsky LS, Saxena SK, Dubrovinskaia NA, Rekhi S, Le Bihan T (2000) *Am Mineral* 85:386–389.
11. Brown JM, Mcqueen RG (1986) *J Geophys Res* 91:7485–7494.
12. Brown JM, Fritz JN, Hixson RS (2000) *J Appl Phys* 88:5496–5498.
13. Stevenson DJ (1981) *Science* 214:611–619.
14. Poirier JP (1994) *Phys Earth Planet Inter* 85:319–337.
15. Hillgren V, Gessmann CK, Li J (2000) in *Origin of the Earth and Moon*, eds Canup R, Righter K (Univ of Arizona Press, Tucson), pp 245–263.
16. Li J, Fei Y (2003) *Treatise on Geochemistry*, ed Carlson RW (Elsevier, New York), Vol 2, pp 21–546.
17. Seagle CT, Campbell AJ, Heinz DL, Shen G (2006) *J Geophys Res* 111:B06209.
18. Guyot F, Zhang J, Martinez I, Matas J, Richard Y, Javoy M (1997) *Eur J Mineral* 9:277–286.
19. Zhang J, Guyot F (1999) *Phys Chem Miner* 26:206–211.
20. Vočadlo L, Knight KS, Price GD, Wood IG (2002) *Phys Chem Miner* 29:132–139.

21. Wood IG, Vočadlo L, Knight KS, Dobson DP, Marshall WG, Price GD, Brodholt J (2004) *J Appl Crystallogr* 37:82–90.
22. Fei Y, Li J, Bertka CM, Prewitt CT (2000) *Am Mineral* 85:1830–1833.
23. Angel RJ (2001) *Rev Miner Geochem* 41:35–60.
24. Lin JF, Heinz DL, Campbell AJ, Devine JM, Shen GY (2002) *Science* 295:313–315.
25. Rama Murthy V, Hall HT (1970) *Phys Earth Planet Inter* 2:276–282.
26. Ahrens TJ (1979) *J Geophys Res* 84:985–998.
27. Dreibus G, Wänke H (1985) *Meteoritics* 20:367–381.
28. Brown JM (2001) *Geophys Res Lett* 28:4339–4342.
29. Jacobs JA (1987) *The Earth's Core* (Academic, London).
30. Dreibus G, Palme H (1995) *Geochim Cosmochim Acta* 60:1125–1130.
31. Allégre CJ, Poirier JP, Humler E, Hoffman AW (1995) *Earth Planet Sci Lett* 134:515–526.
32. Gessmann CK, Wood BJ, Rubie DC, Kilburn MR (2001) *Earth Planet Sci Lett* 184:367–376.
33. McDonough WF, Sun SS (1995) *Chem Geol* 120:223–253.
34. Wänke H, Dreibus G (1997) *Lunar Planet Sci* 28:1495–1496.
35. Hirao N, Ohtani E, Kondo T, Kikegawa T (2004) *Phys Chem Miner* 31:329–336.
36. Williams Q, Knittle E (1997) *Phys Earth Planet Inter* 100:49–59.
37. Wood IG, Chaplin TD, David WIF, Hull S, Price GD, Street JN (1995) *J Phys Condens Matter* 7:L475–L479.
38. Rueff JP, Kao CC, Struzhkin VV, Badro J, Shu J, Hemley RJ, Mao HK (1999) *Phys Rev Lett* 82:3284–3287.
39. Rueff JP, Kao CC, Struzhkin VV, Badro J, Shu J, Hemley RJ, Mao HK (1999) *Phys Rev Lett* 83:3343.
40. Lin JF, Fei Y, Sturhahm W, Zhao JY, Mao HK, Hemley RJ (2004) *Earth Planet Sci Lett* 226:33–40.
41. Lin JF, Struzhkin VV, Mao, H. k., Hemley RJ, Chow P, Hu MY, Li J (2004) *Phys Rev B* 70:212405.
42. Vočadlo L, Brodholt J, Dobson D, Knight K, Marshall W, Price G, Wood I (2002) *Earth Planet Sci Lett* 203:567–575.
43. Fei Y (1996) in *Mineral Spectroscopy: A Tribute to Roger G. Burns*, eds Dyar MD, McCammon C, Shaefer MW (Geochem Soc, Houston), Special Publication No 5, pp 243–254.
44. Toby BH (2001) *J Appl Phys* 34:210–213.
45. Larson A, Dreele RV (2004) *General Structure Analysis System (gsas)* (Los Alamos National Laboratory, Los Alamo, NM), report no LAUR 86-748.
46. Anderson OL, Isaak DG, Yamamoto S (1989) *J Appl Phys* 65:1534–1543.
47. Birch F (1978) *J Geophys Res* 83:1257–1268.
48. Fei Y, Li J, Hirose K, Minarik W, Van Orman J, Sanloup C, vanWestrenen W, Komabayashi T, Funakoshi K-i (2004) *Phys Earth Planet Inter* 143–144: 515–526.